

Production and application of electron vortex beams

J. Verbeeck¹, H. Tian¹ & P. Schattschneider²

Vortex beams (also known as beams with a phase singularity) consist of spiralling wavefronts that give rise to angular momentum around the propagation direction. Vortex photon beams are widely used in applications such as optical tweezers to manipulate micrometre-sized particles and in micro-motors to provide angular momentum^{1,2}, improving channel capacity in optical³ and radio-wave⁴ information transfer, astrophysics⁵ and so on⁶. Very recently, an experimental realization of vortex beams formed of electrons was demonstrated⁷. Here we describe the creation of vortex electron beams, making use of a versatile holographic reconstruction technique in a transmission electron microscope. This technique is a reproducible method of creating vortex electron beams in a conventional electron microscope. We demonstrate how they may be used in electron energy-loss spectroscopy to detect the magnetic state of materials and describe their properties. Our results show that electron vortex beams hold promise for new applications, in particular for analysing and manipulating nanomaterials, and can be easily produced.

It is well known in optics that photons carry angular momentum of $\pm\hbar$ when circularly polarized. This is called spin angular momentum and was demonstrated experimentally by Beth⁸ in 1935. Linearly polarized beams can also carry angular momentum of $l\hbar$ when they have a so-called topological charge² l . This angular momentum is called orbital angular momentum (OAM) and was surprisingly only recently discovered and exploited⁹. A typical demonstration of OAM in optical beams consists of making absorptive particles rotate in the same sense as the angular momentum carried by the beam¹. The discovery of OAM in optics has led to a wide range of applications and many more are expected^{4,5,10}.

Optical beams carrying OAM can be produced with phase plates, computer-generated holograms, spatial light modulators or even by constructing lasers that only emit helical Laguerre–Gaussian modes¹¹. These Laguerre–Gaussian modes have azimuthal helical wave functions given in radial coordinates as:

$$\Psi_{\text{LG}}(r, \varphi) \propto e^{i l \varphi} L(r)$$

where φ is the azimuthal angle, r is the radial coordinate and L is a Laguerre function. l determines the topological charge. Here we demonstrate our ability to transpose this idea to the field of accelerated particle physics by creating OAM in beams of fast electrons.

In addition to their spin, electrons may carry angular orbital momentum, as in atomic bound states. Free electrons, on the other hand, are rarely considered as carrying OAM. We show here how to prepare a free electron that is initially in a plane wave state into an angular-momentum eigenstate. A typical electron beam can be made into a plane wave with wavelength determined by the acceleration voltage, which can be of the order of picometres for acceleration voltages of hundreds of kilovolts.

This plane wave can be converted into an Laguerre–Gaussian beam carrying OAM by using a helical phase plate. This idea has been discussed recently⁷. In practice, however, such a phase plate is very

difficult to produce because it requires a spiralling thickness profile fabricated with nanometre precision. Even if we could make such a phase plate, it would hardly be reproducible and might suffer from contamination and beam damage.

Side effects such as Bragg scattering and thermal diffuse scattering in the material will likewise complicate the situation. The best approach at present available is the macroscopic production of graphite sheets with varying thickness, and then looking for a favourable location on such a sheet, that is, where the stacking of two or more layers comes close to a spiral structure⁷. This approach is also inevitably limited to a low topological charge l in view of the absorption of electrons in a phase plate that otherwise would become too thick. We have therefore chosen a new approach, based on computer-generated holograms.

A computer-generated hologram—as also used in optics^{12,13}—is by far more suitable for electrons, because one can work with a binary mask that either blocks or passes the electrons in specific places. The masks can easily be produced with focused ion beam instruments, and one has complete control over the phase and amplitude of the electron beam.

In order to do so, one specifies a target complex wave function Ψ_t containing OAM:

$$\Psi_t = e^{i l \varphi} f(r)$$

for which we omit the dynamic phase $e^{i k_0 z}$ dependence along the beam propagation direction, with $k_0 = \frac{1}{\lambda}$ the incoming electron wavevector. Interference is created with a reference plane wave that is tilted:

$$\Psi_{\text{ref}} = e^{i 2 \pi k_{\perp} \cdot r_{\perp}}$$

where k_{\perp} is the component of the wavevector that is perpendicular to the incoming wavevector k_0 expressing the tilt. A virtual hologram is then computed as the interference between the target wave and the reference wave:

$$I_{\text{holo}} = |\Psi_t + \Psi_{\text{ref}}|^2$$

This hologram is transformed into a binary mask by clipping.

$$I_{\text{mask}} = \begin{cases} 1 & \Leftrightarrow I_{\text{holo}} > 0.5 \text{ and } r < R_{\text{max}} \\ 0 & \Leftrightarrow \text{elsewhere} \end{cases}$$

and a maximum radius R_{max} is defined. A computer-generated hologram aperture defined like this for $l = 1$ and $k_{\perp} = 4/R_{\text{max}}$ is shown in Fig. 1a, which shows an edge dislocation as already discussed theoretically by Nye¹⁴ for arbitrary waves. The far-field behaviour of this mask when illuminated with a plane wave can be calculated as the Fourier transform shown in Fig. 1b. Because the mask function is real, we observe two sidebands which are each other's complex conjugate and a central band. The two sidebands carry the target angular momentum $l = \pm 1$, while the central beam carries no angular momentum. We note that the production of any topological charge l is, in principle, possible in this way.

¹Electron Microscopy for Materials Science (EMAT), University of Antwerp, Groenenborgerlaan 171, B-2020 Antwerp, Belgium. ²Institute for Solid State Physics and University Service Centre for Electron Microscopy, Vienna University of Technology, A-1040 Vienna, Austria.

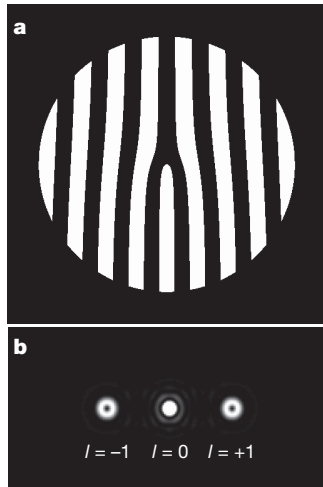


Figure 1 | Calculated holographic reconstruction of a wavefunction carrying angular momentum. **a**, Binary mask. **b**, Theoretical far-field intensity showing two sidebands carrying topological charge $l = \pm 1$.

In a next step, we produce the mask from a thin Pt foil, making use of a dual-beam focused ion beam instrument. We created masks with a diameter of $2R_{\text{max}} = 5 \mu\text{m}$ and $2.5 \mu\text{m}$ in a Pt foil thickness of approximately 100 nm. A scanning electron microscope picture showing the $5\text{-}\mu\text{m}$ mask is given in Fig. 2a.

When this mask is placed in a sufficiently coherent electron beam, we can visualize the far-field behaviour in the focal plane of the electron optical lens system of a transmission electron microscope (a Philips CM30 UT with a field emission gun and accelerating voltage of 300 kV). The observed far-field pattern is shown in Fig. 2b and resembles the theoretical far-field intensity in Fig. 1b very closely. We note that the observation of this far-field pattern also proves that the phase vortex is present for each doughnut-shaped sideband, because only in that case do both mask and observed pattern form a Fourier transform pair. A direct experimental proof of the phase vortex in each sideband is obtained by the Fresnel effect of a sharp slightly defocused ($\Delta z \approx 700 \text{ nm}$ with 300-kV electrons) aperture, similar to the work of ref. 15 for X-rays. This technique is known as inline holography, and in general a simulation is needed to understand how the phase information is transferred into the observed fringe pattern shown in Fig. 3a. A simulation of the fringe pattern shown in Fig. 3b shows that the observed fringe pattern is indeed the signature of two

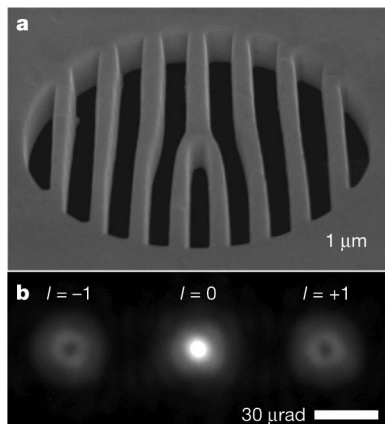


Figure 2 | Experimental realization of the holographic reconstruction technique. **a**, Scanning electron microscope image of a $5\text{-}\mu\text{m}$ phase dislocation aperture made in a thinned Pt foil. **b**, Diffraction pattern obtained in the far field of the vortex aperture when illuminated with a plane wave of 300-kV electrons. The pattern clearly shows the doughnut-shaped sidebands, each carrying opposite angular momentum.

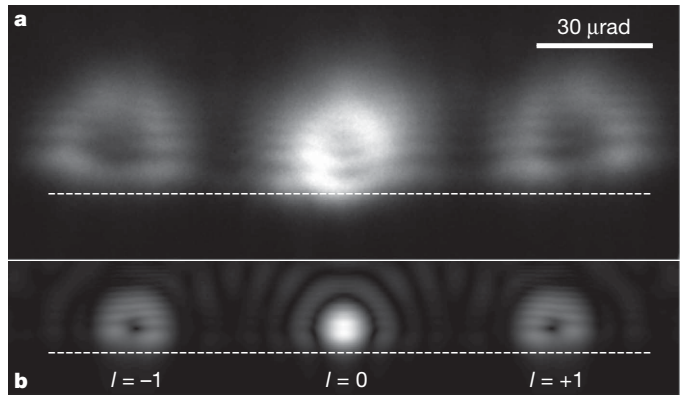


Figure 3 | Experimental proof of the angular momentum in the sidebands. **a**, Experimental Fresnel fringes created by a sharp aperture edge (indicated by a dashed line) showing opposite edge dislocations in the fringe pattern of the two sidebands. A defocus of $\Delta z \approx 700 \text{ nm}$ is used with 300-kV electrons recorded via a scintillator on a charge-coupled device (CCD). **b**, Simulated Fresnel fringes to prove that the phase vortex in both sidebands leads to the observed fringe pattern.

opposite phase vortices with $l = \pm 1$ in the sidebands, whereas the central beam does not show a phase discontinuity.

This demonstrates a new way to prepare an electron beam carrying arbitrary OAM following a relatively simple ‘recipe’. We note that the discretization of the mask leads to higher-order sidebands with multiples of the initial angular momentum $l\hbar$, as shown in more detail in the Supplementary Information.

Having demonstrated the ability to create electron beams carrying OAM efficiently, we discuss some of the properties of these beams, which set them apart from photon vortex beams. A theoretical comparison between electron and photon vortex waves has already been made¹⁶. Most notably, electrons carry charge; have mass and a fractional spin angular momentum of $\pm\hbar/2$. The helical wave fronts define a spiralling quantum mechanical probability current that gives rise to interesting magnetic effects.

Here we demonstrate how these vortex beams can be applied to energy-loss magnetic circular dichroism, a recently established method of studying magnetic circular dichroism in the electron microscope¹⁷. In the standard energy-loss magnetic circular dichroism geometry, spin-polarized $2p_j \rightarrow 3d$ electronic transitions are mapped in angle-resolved energy-loss spectrometry¹⁸. The time-reversal symmetry broken by the external magnetic field induces a slight asymmetry of the energy-dependent inelastic cross-section in the diffraction plane. The asymmetry has opposite sign for the $j = 1/2$ and $j = 3/2$ transitions and is equivalent to the X-ray magnetic circular dichroism effect usually obtained in a synchrotron. In X-ray magnetic circular dichroism, the spin angular momentum of the X-ray photons $\pm\hbar$ is equivalent to the orbital angular momentum of $\pm\hbar$ in our spin unpolarized electron beams. This asymmetry is related to a slight preference of $\Delta m = 1$ over $\Delta m = -1$ dipole transitions via spin-orbit coupling (or vice versa, the inelastic cross-section must be different for incident electron beams with $L_z = \pm 1$). That is, a thin ferromagnetic film in the specimen plane of Fig. 4a serves as a chiral filter for the $l = 1/l = -1$ vortices when observing the energy-loss spectrum, analogous to a polarizer/analyser combination in optics. It should be noted that the effect hinges on a slight defocus z between the mask and the image plane of the specimen, as indicated in Fig. 4a. This defocus creates a coherent patch in the plane of the binary mask that enables it to act as a chiral analyser.

In more technical terms, transitions from a core state to a final unoccupied state are typically determined by spherical harmonic matrix elements that can provide OAM to the inelastically scattered fast electrons¹⁹. Taking into account the generalized reciprocity theorem²⁰ (stating that the order of polarizer and sample can be exchanged for inelastic scattering) and making use of the holographic mask, we can now detect

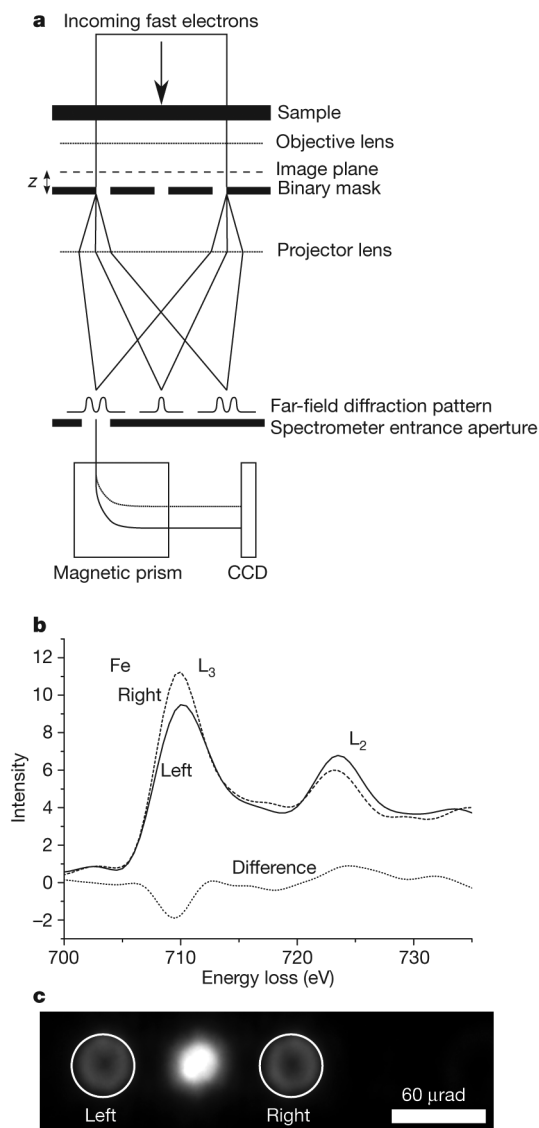


Figure 4 | Application of the vortex beam to EELS. **a**, Sketch of the set-up. The spectrometer is placed on either the left or right sideband, and a defocus of $z \approx 750$ nm is applied between the sample and the binary mask. **b**, Fe $L_{2,3}$ EELS signal obtained in the left and right sideband showing clear differences due to chiral selection rules. The sample is 50-nm-thick homogeneously magnetized ferromagnetic body-centred cubic Fe and shows clear dependence of the signal on the chirality of the transition. **c**, Far-field diffraction pattern showing the position of the 40- μ rad spectrometer entrance aperture for the left and right sidebands.

the OAM of the inelastically scattered coherent partial wave emitted from a scattering centre in a way equivalent to probing excitations with circularly polarized X-ray beams in X-ray magnetic circular dichroism. Indeed, if a spectrometer is set up to determine the energy of the electrons in either the left ($l = -1$) or right ($l = +1$) sideband, one achieves a discrimination for transitions with the two symmetries $e^{im\phi}$. This is because a selection rule applies that only allows transitions for which $l + m = 0$. (The condition $l + m = 0$ states that the angular momentum of the closed system is a constant of motion.)

The resulting Fe L_2 and L_3 (with L_2 and L_3 indicating a $2p_{1/2} \rightarrow 3d$ and $2p_{3/2} \rightarrow 3d$ transition) spectra are shown in Fig. 4b. The collection angle was 40 μ rad (shown in the far-field pattern in Fig. 4c), slightly defocused to $z \approx 750$ nm, and the exposure time was 60 s. The energy resolution was 0.7 eV and the effective diameter of the region of the sample participating in the spectra is approximately 250 nm. The Fe sample is homogeneously magnetized along the optical axis by the magnetic field of the objective lens and has an approximate thickness

of 50 nm. The difference spectrum shown in Fig. 4b is also known as the energy-loss magnetic circular dichroism spectrum¹⁷. It shows the typical characteristics of spin-polarized transitions in ferromagnetic materials (also known from X-ray magnetic circular dichroism experiments). Changing the sign of the magnetization direction in X-ray magnetic circular dichroism would be identical to changing the order in which we subtract both spectra.

This experiment demonstrates both the vortex nature of the electron beams produced by the holographic mask, and the usefulness of electron vortex beams in the study of chirality in inelastic transitions. In comparison to the standard method of obtaining energy-loss magnetic circular dichroism spectra¹⁷, we expect a much higher signal-to-noise ratio and the possibility of using these vortex beams (in a different set-up, as presented here) for atomic resolution scanning with magnetic sensitivity. Theoretical simulations of such a set-up show an improvement of the discrimination between $\Delta m = \pm 1$ transitions by a factor of ten as compared to the standard geometry, opening the road for mapping the local magnetic state in materials with atomic resolution in a transmission electron microscope.

Holographic OAM beams of fast electrons should allow many new applications in fundamental and in applied physics. A possible experiment would be a variant of the Aharonov–Bohm effect when creating interference between the left and right sidebands¹⁶. The magnetic effect could potentially serve to create electronic tweezers holding atoms in the centre of the doughnut-shaped beam, with diameters of the order of a few atoms. Similarly to the focused ion beam technique, vortex beams could open new possibilities for nano-patterning. The transfer of angular momentum mediated by the torque of the spiralling Poynting vector²¹ can accelerate nanoparticles to a spinning rate close to centrifugal decomposition²², certainly revealing new interesting physics. Superposition of the two sidebands (for example, by a biprism or a crystal beam splitter) creates fast electrons with p -symmetry, having potential applications for the study of directional bonds in electron energy-loss spectroscopy (EELS).

Received 7 May; accepted 16 July 2010.

1. He, H., Friese, M. E. J., Heckenberg, N. R. & Rubinsztein-Dunlop, H. Direct observation of transfer of angular momentum to absorptive particles from a laser beam with a phase singularity. *Phys. Rev. Lett.* **75** (5) 826–829 (1995).
2. O’Neill, A. T., Mac Vicar, I., Allen, L. & Padgett, M. J. Intrinsic and extrinsic nature of the orbital angular momentum of a light beam. *Phys. Rev. Lett.* **88** (5) 053601 (2002).
3. Barreiro, J. T., Wei, T.-C. & Kwiat, P. G. Beating the channel capacity limit for linear photonic superdense coding. *Nature Phys.* **4**, 282–286 (2008).
4. Thidé, B. *et al.* Utilization of photon orbital angular momentum in the low-frequency radio domain. *Phys. Rev. Lett.* **99**, 087701 (2007).
5. Berkhout, G. C. G. & Beijersbergen, M. W. Using a multipoint interferometer to measure the orbital angular momentum of light in astrophysics. *J. Opt. A* **11**, 094021(7) (2009).
6. Franke-Arnold, S., Allen, L. & Padgett, M. Advances in optical angular momentum. *Laser Photon Rev.* **2**, 299–313 (2008).
7. Uchida, M. & Tomomura, A. Generation of electron beams carrying orbital angular momentum. *Nature* **464**, 737–739 (2010).
8. Beth, R. A. Direct detection of the angular momentum of light. *Phys. Rev.* **48**, 471 (1935).
9. Allen, L., Beijersbergen, M. W., Spreeuw, R. J. C. & Woerdman, J. P. Orbital angular momentum of light and the transformation of Laguerre-Gaussian laser modes. *Phys. Rev. A* **45** (11) 8185–8189 (1992).
10. Cojoc, D. *et al.* X-ray vortices with high topological charge. *Microelectron. Eng.* **83**, 1360–1363 (2006).
11. Beijersbergen, M. W. & Allen, L. van der Veen, H. E. L. O. & Woerdman, J. P. Astigmatic laser mode converters and transfer of orbital angular momentum. *Opt. Commun.* **96**, 123–132 (1993).
12. Bazhenov, V. Y., Vasnetsov, M. V. & Soskin, M. S. Laser beams with screw dislocations in their wavefronts. *JETP Lett.* **52** (8) 429–431 (1990).
13. Heckenberg, N. R., McDuff, R., Smith, C. P., Rubinsztein-Dunlop, H. & Wegener, M. J. Laser-beams with phase singularities. *Opt. Quantum Electron.* **24** (9), S951–S962 (1992).
14. Nye, J. F. & Berry, M. V. Dislocations in wave trains. *Proc. R. Soc. Lond. A* **336**, 165–190 (1974).
15. Peele, A. G. *et al.* Observation of an X-ray vortex. *Opt. Lett.* **27** (20) 1752–1754 (2002).
16. Bliokh, K. Y., Bliokh, Y. P., Savel’ev, S. & Nori, F. Semiclassical dynamics of electron wave packets with phase vortices. *Phys. Rev. Lett.* **99**, 190404 (2007).

17. Schattschneider, P. *et al.* Detection of magnetic circular dichroism using a transmission electron microscope. *Nature* **441**, 486–488 (2006).
18. Rubino, S. *et al.* Energy-loss magnetic chiral dichroism (EMCD): magnetic chiral dichroism in the electron microscope. *J. Mater. Res.* **23** (10) 2582–2590 (2008).
19. Schattschneider, P. *et al.* Real space maps of magnetic moments on the atomic scale: theory and feasibility. *Ultramicroscopy* **110** (8) 1038–1041 (2010).
20. Findlay, S. D., Schattschneider, P. & Allen, L. J. Imaging using inelastically scattered electrons in CTEM and STEM geometry. *Ultramicroscopy* **108** (1) 58–67 (2007).
21. Babiker, M., Power, W. L. & Allen, L. Light-induced torque on moving atoms. *Phys. Rev. Lett.* **73**, 1239–1242 (1994).
22. Garcia de Abajo, F. J. Optical excitations in electron microscopy. *Rev. Mod. Phys.* **82**, 209–275 (2010).

Supplementary Information is linked to the online version of the paper at www.nature.com/nature.

Acknowledgements: J.V. acknowledges financial support from the European Union under the Framework 6 programme under a contract for an Integrated Infrastructure Initiative (reference O26019 ESTEEM). H.T. acknowledges the FWO-Vlaanderen for financial support under contract number G.0147.06.

Author contributions: J.V. developed the idea, designed the apertures, simulated the EELS behaviour, and did first experiments. H.T. did more elaborate experiments and recorded the EELS results. P.S. developed the background of using angular momentum in TEM and EELS and interpreted the results.

Author Information Reprints and permissions information is available at www.nature.com/reprints. The authors declare no competing financial interests. Readers are welcome to comment on the online version of this article at www.nature.com/nature. Correspondence and requests for materials should be addressed to J.V. (jo.verbeeck@ua.ac.be).